INTERNATIONAL JOURNAL FOR NUMERICAL METHODS IN FLUIDS, VOL. 9, 1121–1143 (1989)

ALGEBRAIC TURBULENCE MODELS FOR THE COMPUTATION OF TWO-DIMENSIONAL HIGH-SPEED FLOWS USING UNSTRUCTURED GRIDS

PHILIPPE ROSTAND

INRIA–Menusin, BP105, 78153 Le Chesnay Cedex, France

SUMMARY

The incorporation of algebraic turbulence models in a solver for the 2D compressible Navier–Stokes equations using triangular grids is described. A practical way to use the Cebeci–Smith model and to modify it in separated regions is proposed. The ability of the model to predict high-speed perfect-gas boundary layers is investigated from a numerical point of view.

KEY WORDS Turbulence High-speed flows Unstructured grids

1. INTRODUCTION

Solving the laminar compressible Navier–Stokes equations numerically for practical configurations is now within reach.[1,2] Flows around complete aircraft, including an impressive high-Mach-number flow around a shuttle,[3] have been successfully computed. However, the complexity of the configurations of industrial interest makes these computations a challenging task, even when using modern supercomputers. The results obtained are for steady and laminar flows and still make full use of the computer capability available. This, together with the concern of affordability, is why cost is the major issue when more realistic physical models are taken into account. It is well known that most configurations of interest are at least locally turbulent, and that the modelling of this turbulence is critical for the reliability of the computations. Thus a cheap and reasonably accurate turbulent closure model is an unavoidable part of a compressible viscous code.

The study of the second part of the re-entry of the European shuttle Hermes prompts interest in high-speed moderate Reynolds flows. With Mach numbers ranging from 5 to 10, real-gas effects can be neglected in a first approximation. The purpose of the study is not to predict the details of the flow, which are probably beyond reach anyway, but to give reasonable estimates (say $\pm 10\%$) of the pressure, friction and heat transfer, and, through these, of the flight performance of the shuttle.

An implicit algorithm to solve the 2D (3D) compressible Euler equations on unstructured triangular (tetrahedral) grids has been developed in recent years.[4,5] It is based on a finite volume approximation of the equations in conservation form, using control volumes defined by the medians of the triangle (tetrahedron) surrounding each node, and Osher's flux formula.[6] It has been extended to solve the Reynolds-averaged Navier–Stokes equations and shown to be able to compute two-dimensional laminar boundary layers efficiently and accurately.[7] The purpose of this work is to include in it some relevant turbulence model.

0271–2091/89/091121–23$11.50

Received 10 November 1988

Our concern here will be two-dimensional compressible boundary layers and compression corners, which are the two relevant simple flows (see Figure 1). Numerous turbulence models have been proposed to solve these problems, and a review would make a (tough) paper by itself. However, they can be classified by the number of extra PDEs they introduce, by the order of the closing relation and by its linearity, i.e. by whether the model is of the eddy viscosity type or not. Non-linear models have been shown to be an improvement over linear ones in a number of situations (see e.g. Reference 8), but they will not be our concern here, since we restrict ourselves to two-dimensional situations in this first approach.

The choice is then on the number of PDEs one wishes to solve; it is our opinion that one- and two-equation models offer no significant improvement over algebraic models for computations of the near-wall flows which are our concern. Consequently, we will restrict ourselves to algebraic models, in which we may later introduce some streamwise history effect through an explicit relaxation model, patterned after that of Shang and Hankey.[9] For attached flows the models of Cebeci and Smith[10] and of Baldwin and Lomax[11] have been extensively tested and shown to perform well in the incompressible, transonic and supersonic regimes.[12,13] The Baldwin–Lomax model has the advantage that it does not require calculation of the boundary layer thickness and has been widely used and tested. However, for detached or near-detachment boundary layers, both the Cebeci–Smith and the Baldwin–Lomax models give erroneous results; this is due to the fact that they both rely on Prandtl's mixing-length theory, which is no longer relevant after detachment. In separated regions we will use another algebraic model, introduced by Goldberg,[14] which prescribes analytically the values of k and ε in a separation bubble.

All these models have been previously used and validated. The aim of this paper is twofold. First, we want to show that turbulent flows can be efficiently calculated on unstructured grids using algebraic models; this is not straightforward because the direction normal to the wall is no

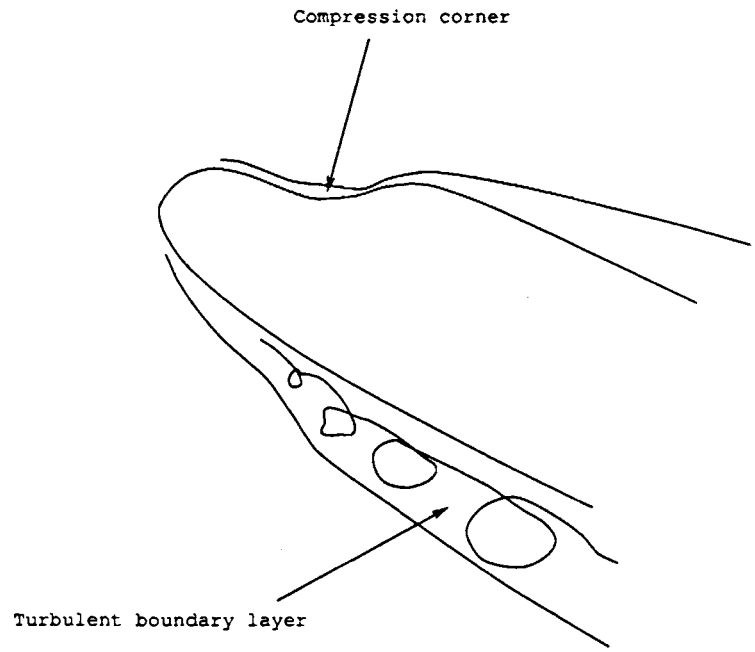

Figure 1

longer a co-ordinate axis, so that non-local effects are not easy to compute. The details of the implementation are given in Section 2. Secondly, we want to investigate how well these algebraic models, which were defined after incompressible theories and thus ignore density fluctuations, will perform for high-speed flows. In Section 3 we will compute a boundary layer at Mach 7·4 and compare the results with the experiments of Hopkins *et al.*[15] No data on hypersonic flows over compression corners are known to the author; however, such a high-speed computation part of the Hermes workshop[16] will be performed in Section 4.

2. ALGEBRAIC TURBULENCE MODELS AND UNSTRUCTURED GRIDS

Linear algebraic turbulence models describe the Reynolds turbulent stress tensor σ_t as

$$\sigma_t = \mu_t D(u) \tag{1}$$

and the turbulent heat flux q_t as

$$q_t = \frac{\mu_t}{Pr_t} \nabla T, \tag{2}$$

where Pr_t is the turbulent Prandtl number, usually assumed constant, and μ_t is the eddy viscosity, which is an explicit function of the flow variables $\mathbf{W}$, although this function is usually not local. More precisely,

$$\mu_t(x_0, y_0) = f(\mathbf{W}(x_0, y), y \geq 0). \tag{3}$$

The value of μ_t at a given point depends on the flow variables at all the points at the same streamwise location.

One of the main advantages of algebraic models, which makes them so popular, is their minimum requirement of computer time and storage. Indeed, when one uses an i, j grid (Figure 2), the value of the eddy viscosity on the grid, μ_{ij}, can be calculated cheaply since

$$\mu_{t i_0 j_0} = f(\mathbf{W}_{i_0 j}, j \geq 0), \tag{4}$$

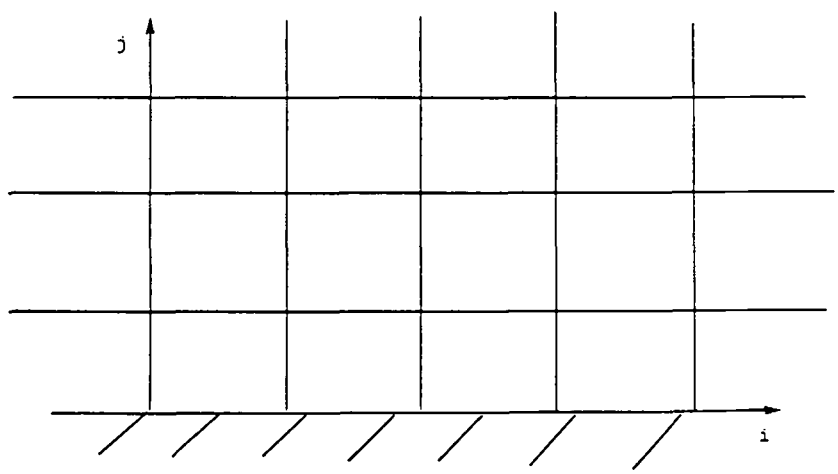

Figure 2

and in (4) many terms in $\mu_{t_{i_0 j_0}}$ are common to all points at same streamwise location and so can be computed only once for each value of i_0.

Whether these desirable features can be conserved for triangular grids, which can be of type (a) but also of type (b) (Figure 3), is the question that must be answered.

A triangular grid can be, and usually is, at least locally, not orthogonal to the wall. In our approximation[7] the flow variables are linear on each triangle, and consequently we will look for nodal values of the eddy viscosity. The normals to the wall cannot, as in the rectangular structured case, be approximated by a sequence of nodes. There are two ways to calculate the field of eddy viscosities. The first is, for each node, to draw the normal to the wall passing through this node, to track all the elements it gets through (Figure 4) and then, using flow variables which are piecewise linear on this normal, to compute the eddy viscosity, which is valid only for the considered node since it is the only node with this streamwise location. This is very expensive, both in storage—since the list of the elements used for each node must be stored, unless it is recalculated at each time step, leading to an enormous CPU cost—and in CPU time—since a complete viscosity calculation on a normal must be performed for each node.

The other way, which we will use, is to consider a discrete set of normals, namely the normals to the wall, passing through the middle of the wall edges (Figure 5), to compute and store the elements they get through, together with the barycentric co-ordinates of the middle of their

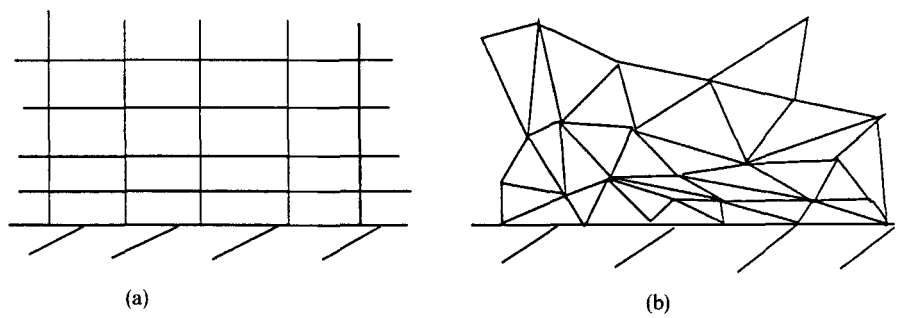

Figure 3

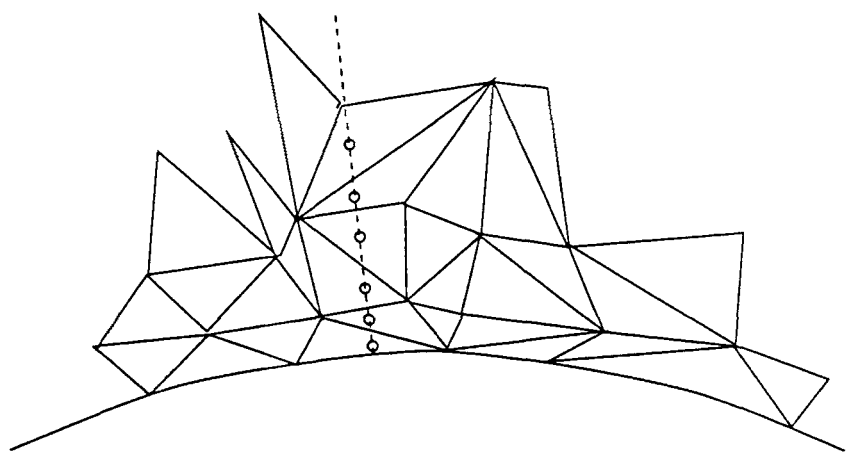

Figure 4

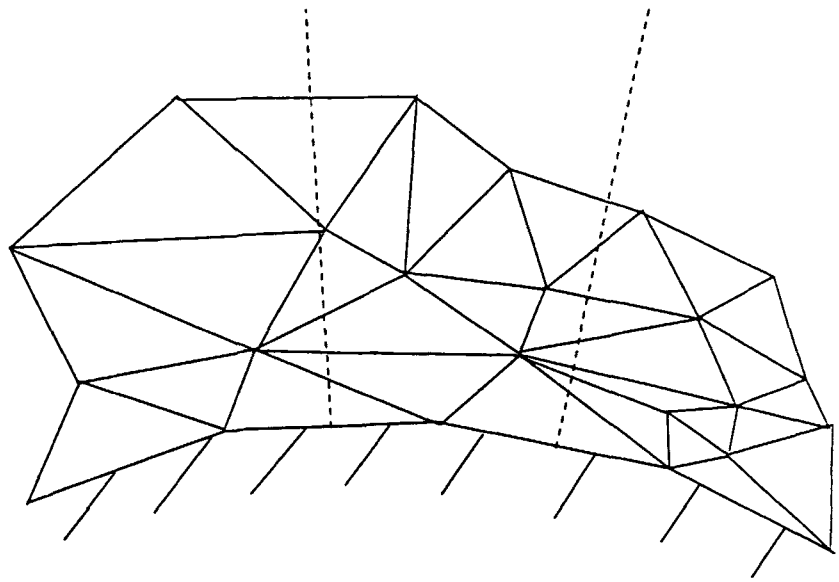

Figure 5

intersection with each element, and then, at each time step, to use that information to compute the eddy viscosity on each normal. For each node it is then necessary to interpolate the values of the eddy viscosity from the two neighbouring normals (Figure 5).

More precisely, the path, in terms of elements and edges, followed by the normal is computed through an algorithm first derived for characteristic methods,[17] taking into account all the geometrical possibilities: the normal hitting a node, coinciding with an edge, etc. This is done once at the beginning of the calculation; the result, which consists, for each wall edge, of a list of triangles and of the barycentric co-ordinates of the middle of the intersection of the normal with each triangle, is stored. The memory needed for this is equal to the number of wall edges multiplied by the average length of a normal (which is fixed by an *a priori* bound to the boundary layer thickness), times one integer (the number of the element) and two reals (the co-ordinates):

$$\text{Sto1} = (\text{wall edges}) \times (\text{average normal length}) \times (1I + 2R). \tag{5}$$

To be able to perform the interpolation of the eddy viscosities from the normals to the whole mesh efficiently, one must also store some geometrical quantities. For each node in the boundary layer, one must store the number of the normal just on its left (say), its distance to this normal, plus one integer and one real to allow positioning on this normal, and one integral and one real to allow positioning on the normal on the right (Figure 6).

Altogether, the memory needed to store the interpolation data is three integers and three reals for each of the nodes in the boundary layer:

$$\text{Sto2} = (\text{boundary layer nodes}) \times (3I + 3R). \tag{6}$$

The global storage needed for the turbulence is

$$\begin{aligned} \text{Sto} = {} & (\text{wall edges}) \times (\text{average normal length})(1I + 2R) \\ & + (\text{boundary layer nodes})(3I + 3R). \end{aligned} \tag{7}$$

For example, a flat plate calculation using 100 nodes on the wall and an average of 25 nodes in the

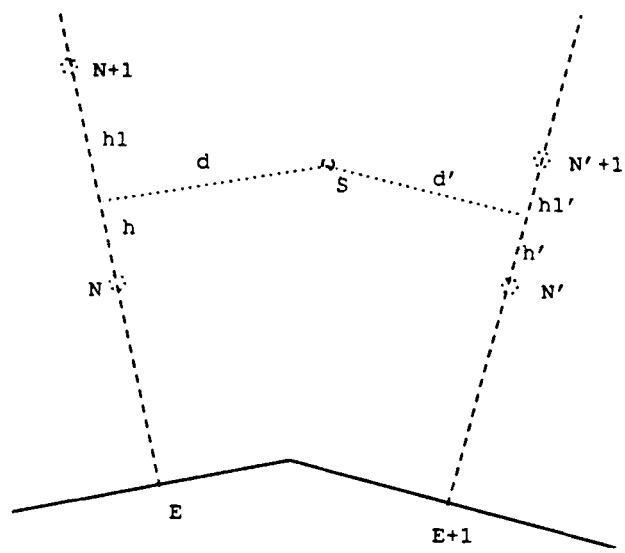

Figure 6

boundary layer will require 90 kbytes of storage for the turbulence data, which is quite reasonable. The generation of these data takes about 40 s on a SUN workstation for this case.

Once these data are generated, at each time step, the eddy viscosity is evaluated on the normals. This is now straightforward, since we have a normal represented by a set of points at which the flow properties, including the vorticity, are known: we are brought back to the structured orthogonal case. Then the interpolation is performed, which is also straightforward, since all the required coefficients are stored. Altogether, the calculation of the eddy viscosity when one uses the Baldwin–Lomax model takes less than 1·5% of the global CPU time for an implicit scheme and less than 4% for an explicit scheme. The evaluation of the eddy viscosity for the aforementioned case takes about 1·2 s on a SUN.

The interpolation procedure described earlier is valid only when the solid body is convex. When it is not, a given point of the flow field is usually considered as influenced by two or more walls, and the influences are proportional to the inverse of the distance to the wall. A similar interpolation can be performed. The only added storage is: one real for each node of the boundary layer, representing the ratio of the influence of the eventual two relevant walls, and in Sto2 a boundary layer node must be counted twice if it is influenced by two convex components of the wall. This can be handled in a completely automatic and geometry-independent way, which is consistent with the finite element spirit.

Although the geometrical part will be much more complicated, the same thing can be done in three dimensions. Normals are drawn starting from the wall faces, and then a spatial interpolation is performed between these normals.

3. HIGH-SPEED ATTACHED BOUNDARY LAYERS

Turbulent boundary layers have been studied quite extensively in the last two decades and described in much detail.[10] Many authors have proposed turbulent closure models to predict these boundary layers. The simpler ones, which will be our concern, are those which suppose the turbulent stress tensor $-\rho\overline{u'v'}$ to be proportional to the deformation tensor D:

$$-\rho\overline{u'v'} = \sigma_t = \mu_t D(u), \tag{8}$$

where μ_t is the eddy viscosity, which in algebraic models is a function of the flow field.

Many eddy viscosity laws $\mu_t = \mu_t(\mathbf{W})$ have been proposed over the years; the successful ones separate the boundary layer into an inner and an outer part which behave differently. In the inner part the main feature of the analysis is Prandtl's mixing-length theory, which predicts the eddy viscosity to be

$$\mu_t = \rho l^2 |\omega|, \tag{9}$$

where $|\omega|$ is the magnitude of the vorticity and l the mixing length. According to Prandtl's theory, in the fully turbulent regime l is proportional to the distance to the wall:

$$l = \kappa y. \tag{10}$$

To account for the laminar sublayer, this expression has to be modified in the near-wall region, as we will see later on.

In the outer part of the boundary layer, it is generally admitted that the eddy viscosity is almost constant, although different values of this constant have been proposed. Cebeci and Smith[10] suppose that

$$\mu_t = \alpha u_e \delta_i, \tag{11}$$

where α is Clauser's constant, u_e the speed at the edge of the boundary layer and δ_i the incompressible displacement thickness. Again, this expression must be modified when approaching the edge of the boundary layer to account for the relaminarization of the flow.

From these ideas, Cebeci and Smith proposed an eddy viscosity model defined as

$$\mu_t = \rho l^2 |\omega|, \qquad l = xy[1 - \exp(-y/A)], \qquad y \leqslant y_c, \tag{12}$$

$$\mu_t = \alpha u_e \delta_i \gamma, \qquad \gamma = [1 + 5{\cdot}5(y/\delta)^6]^{-1}, \qquad y \geqslant y_c, \tag{13}$$

where $1 - \exp(-y/A)$ is Van Driest's damping factor, which allows the representation of the laminar sublayer. A is the damping length, which according to Cebeci and Smith is given by

$$A = A^+ \mu / \sqrt{(\rho \tau_w)}, \qquad A^+ = 26. \tag{14}$$

γ is Klebanoff's intermittency factor, which accounts for the alternately turbulent and laminar regime which occurs around the boundary layer edge. It has been established experimentally by Klebanoff.[18] The crossover value y_c is obtained by requiring the continuity of μ_t.

This model has been tested extensively by its authors and shown to perform well in the incompressible, subsonic and transonic cases. Its main drawback is the necessity to first define and then calculate the boundary layer edge location and the properties of the flow at that point, in order to calculate the outer eddy viscosity. This is very difficult to do numerically with a reasonable accuracy.

To overcome this difficulty, Baldwin and Lomax[11] proposed an alternative outer formulation

$$\mu_t = \alpha C_{cp} \rho Y_{MAX} F_{MAX} \gamma, \qquad y \geqslant y_c, \tag{15}$$

where

$$F(y)=y|\omega|[1-\exp(-y/A)], \tag{16}$$

F_{MAX} is the maximum of F in a profile and Y_{MAX} is the value of y at which it takes place. They take

$$\delta = Y_{MAX}/C_{KL}, \tag{17}$$

where C_{cp} and C_{KL} are constants determined by (17) and

$$C_{cp}Y_{MAX}F_{MAX}=u_e\delta_i \tag{18}$$

for theoretical profiles. York and Knight[13] have shown that although the values $C_{cp}=1{\cdot}2$ and $C_{KL}=0{\cdot}65$ could be used for low-speed flows, for high speed flows these values depended very strongly not only on the Mach number but also on the skin friction, making the model quite unreliable. Another difficulty of the model is that for high speeds the function $F(y)$ does not exhibit a sharp peak as in the transonic case,[11] making the determination of Y_{MAX} and F_{MAX} difficult and unreliable.

As remarked before, the difficulty involved in using the Cebeci–Smith model comes from the necessity to find u_e, δ_i and δ. We have

$$\delta_i=\int_0^\delta\left(1-\frac{u}{u_e}\right)dy, \qquad u_e\delta_i=\int_0^\delta(u_e-u)\,dy. \tag{19}$$

It is clear that an inaccurate determination of δ and $u_e=u_e(\delta)$ will result in a very inaccurate value of the eddy viscosity. However, integrating (19) by parts, we have

$$u_e\delta_i=\int_0^\delta y\frac{\partial u}{\partial y}dy,$$

which for an attached flow is equivalent to

$$u_e\delta_i=\int_0^\delta y|\omega|\,dy. \tag{20}$$

For high-Reynolds-number flows, the vorticity $|\omega|$ always decreases sharply as the distance to the wall increases, even when the boundary layer experiences pressure gradients or interaction with a shock. The function $y|\omega|$ also decreases quite quickly, as we will see in the numerical results, so that to calculate $u_e\delta_i$ using (20), we only need a rough estimate of δ. We obtain this estimate through the variations of the Baldwin–Lomax function F: we stop the integration in (20) at the point y^* where $F(y^*)$ is lower than $F^*_{MAX}\beta$, where β is an arbitrary constant. Since the function $y|\omega|$ decreases quite quickly, $\beta=0{\cdot}5$ gives an accurate enough result and allows us to separate between the boundary layer and an eventual shock:

$$u_e\delta_i=\int_0^{y^*}y|\omega|\,dy. \tag{21}$$

To calculate the intermittency factor γ, we need a more accurate estimate of δ. We define a scaling length by

$$y_{av}=\int_0^{y^*}y^2|\omega|\,dy\Big/\int_0^{y^*}y|\omega|\,dy. \tag{22}$$

By comparison with the theoretical profiles of Sun and Childs,[19] it is found that

$$\delta = y_{av}/C_{KL}, \tag{23}$$

where C_{KL} is a constant which depends only slightly on the flow parameters (see Figure 7) and which can be taken to be

$$C_{KL}=0{\cdot}45 \tag{24}$$

for all practical purposes.

In the original Baldwin–Lomax model the damping length A was calculated using only wall quantities:

$$A=A^{+}\mu_w/\sqrt{(\rho_w\tau_w)}.$$

There is no significant difference between this and (14) for low Mach numbers because the density and molecular viscosity do not vary much, but for high speed flows there is a difference, and the Cebeci–Smith expression (14) is found to give better results.

Finally, the model we are using for zero-pressure-gradient boundary layers is μ_t given by (12) in the inner layer, with the damping length given by (14), and in the outer layer

$$\mu_t=\alpha u_e\delta_i\gamma, \tag{25}$$

with $u_e\delta_i$ given by (21) and

$$\gamma=[1+5{\cdot}5(C_{KL}y/y_{av})^6]^{-1}, \tag{26}$$

where the length scale y_{av} is given by (32).

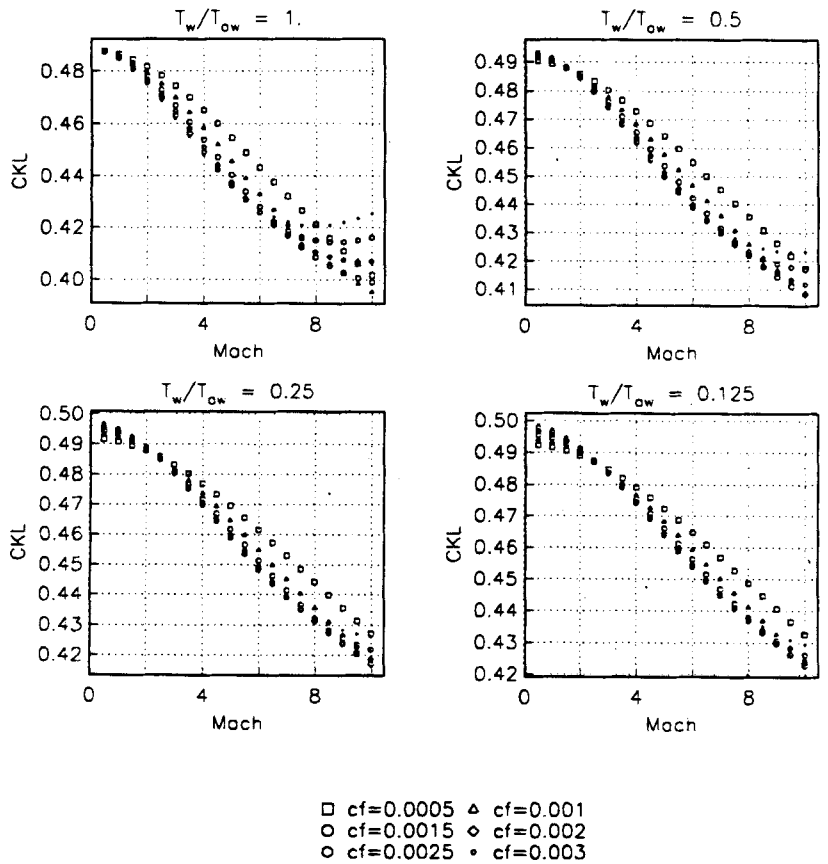

Figure 7. Variations of C_{KL} with the flow parameters

Two high-speed flows over flat plates were computed and the results were compared with the experimental data of Hopkins *et al.*[15] Unfortunately, high-speed measurements are quite scarce and only skin friction values were available. The first case is a flow at $M_\infty = 7{\cdot}4$ and $Re_\infty/m = 8 \times 10^6$. The plate has a length of 2 and a height of 0·35. The grid has 2960 nodes and 5688 elements (Figure 8); it was generated by splitting the quadrangles of a 74×40 grid through their diagonal. The shock is captured at the leading edge. The free stream temperature is $T_\infty = 97{\cdot}3$ K, while the temperature at the wall is $T_w = 311$ K, which is about one-third of the adiabatic temperature. The molecular viscosity is given by Sutherland's law.

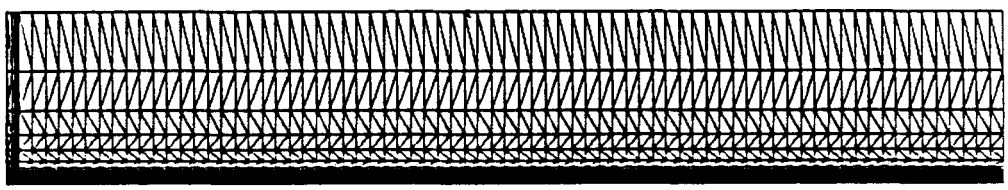

Figure 8

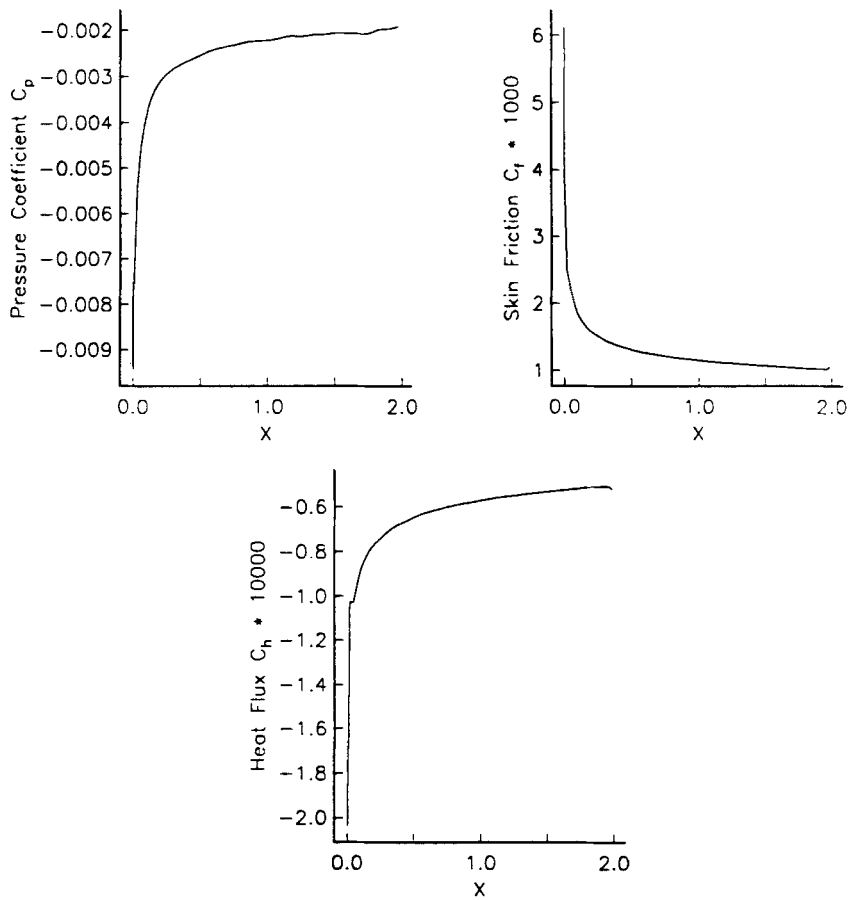

Figure 9

Figure 9 shows the pressure coefficient, skin friction and heat flux versus the streamwise coordinate x. The capturing of the shock is done sharply, as one can see from the low deviation of the pressure coefficient (less than 1%) (the leading edge is at $x=0$). The skin friction and heat flux have the expected behaviour, starting at very high values and decreasing sharply as the Reynolds number $Re_x = Re_w x$ increases. The temperature of the wall is lower than the adiabatic temperature, so that the heat is transferred from the flow to the wall. In Figure 10 the skin friction is plotted against the momentum Reynolds number and compared with the data of Hopkins *et al.* The agreement is very good except for the first point, at $Re_\theta = 800$, which is in transitional flow; no attempt to account for the transition has been made here. The streamwise variations of θ, $u_e\delta_i$ and Y_{av} are also presented. It can be seen that they are very smooth, although a few discontinuities appear near the end of the plate, where the higher and coarser part of the grid plays a role. The crosswind profiles at $x = 1{\cdot}45$ of the speed, the density, the turbulent and total shear stress and ωy are presented in Figure 11. Although no experimental data were available for comparison, the

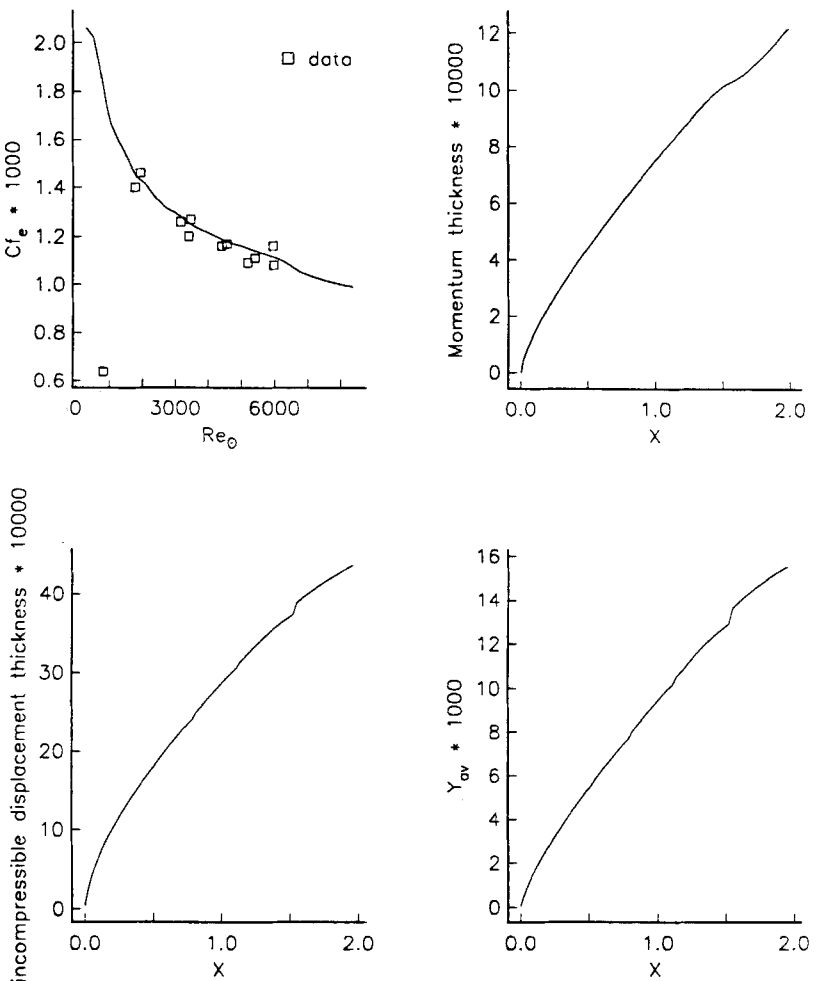

Figure 10

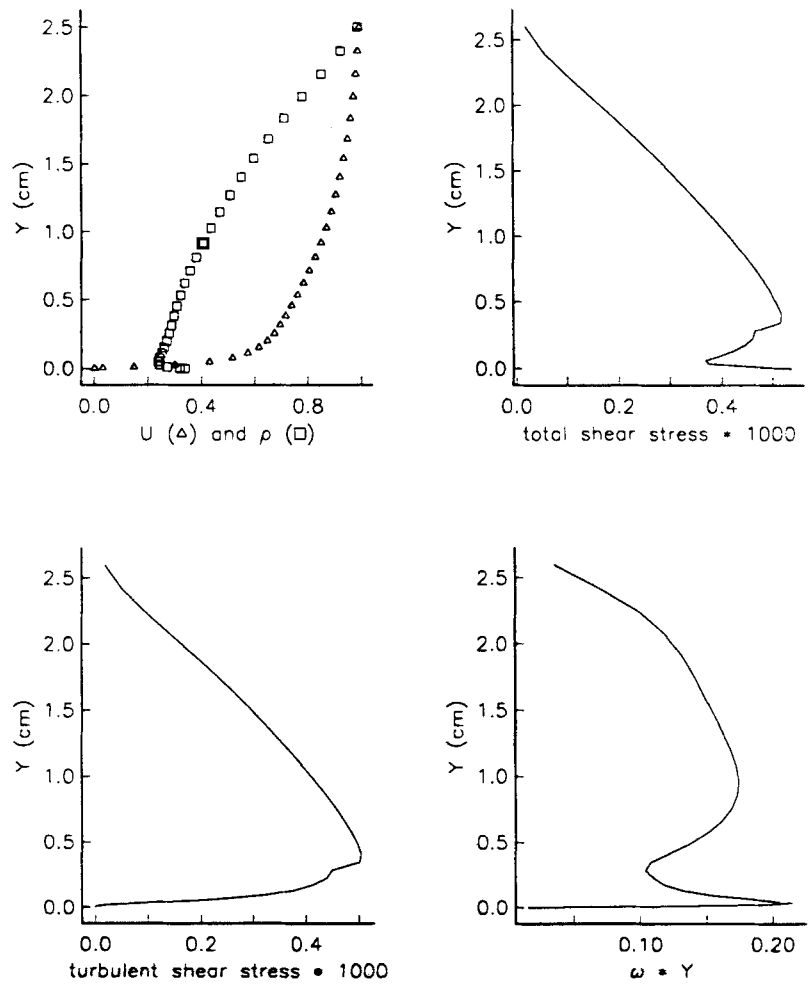

Figure 11

results are quite reasonable, at least qualitatively. The density profile exhibits a minimum short of the wall; this is consistent with the fact that the wall is colder than the corresponding adiabatic wall. This density peak induces a peak in the total shear stress because the eddy viscosity is proportional to the density. This behaviour is maybe not physical and is a drawback of the mixing-length theory. We have checked that it is not dependent on whether local or wall flow properties are used in the calculation of the damping length. As stated before, the function ωy decreases quite quickly when approaching the boundary layer edge and can be integrated easily with a reasonable accuracy. This computation took about 10 h of CPU time on a Gould, of which only about 3% was due to the evaluation of the eddy viscosity. The main overcost when compared to laminar calculations comes from the slower convergence to steady state. The resolution algorithm is a linearly implicit pseudo-time marching to steady state, in which the variations of the eddy viscosity with respect to time are not taken into account: at time level n the viscosity is frozen and the algorithm is advanced by one time step, giving the flow properties at time $n+1$ at which

the eddy viscosity is re-evaluated. This still allowed the use of a Courant number of 50 without encountering stability problems, but the number of iterations necessary to converge to steady state was about 50% more than in the laminar case, giving a 50% overcost.

Another of the test cases of Hopkins *et al.*, at a higher wall temperature, was computed. The geometry is the same as previously; the Mach number is $M_\infty = 7{\cdot}4$, the Reynolds number is $Re_\infty/m = 3 \times 10^7$, the free stream temperature is $T_\infty = 58$ K and the wall temperature is $T_w = 305$ K. The grid used has 1170 nodes and 2204 elements; it was obtained by splitting a 30×39 grid into triangles. In Figures 12–14 the same results as for the previous case are presented. Because of the much coarser streamwise discretization, the results are less smooth and the agreement with experimental data is not as good as for the previous case. Nevertheless, the error in the skin friction (about 8% at the maximum) is less than the estimated experimental error, so that the agreement can be considered reasonable.

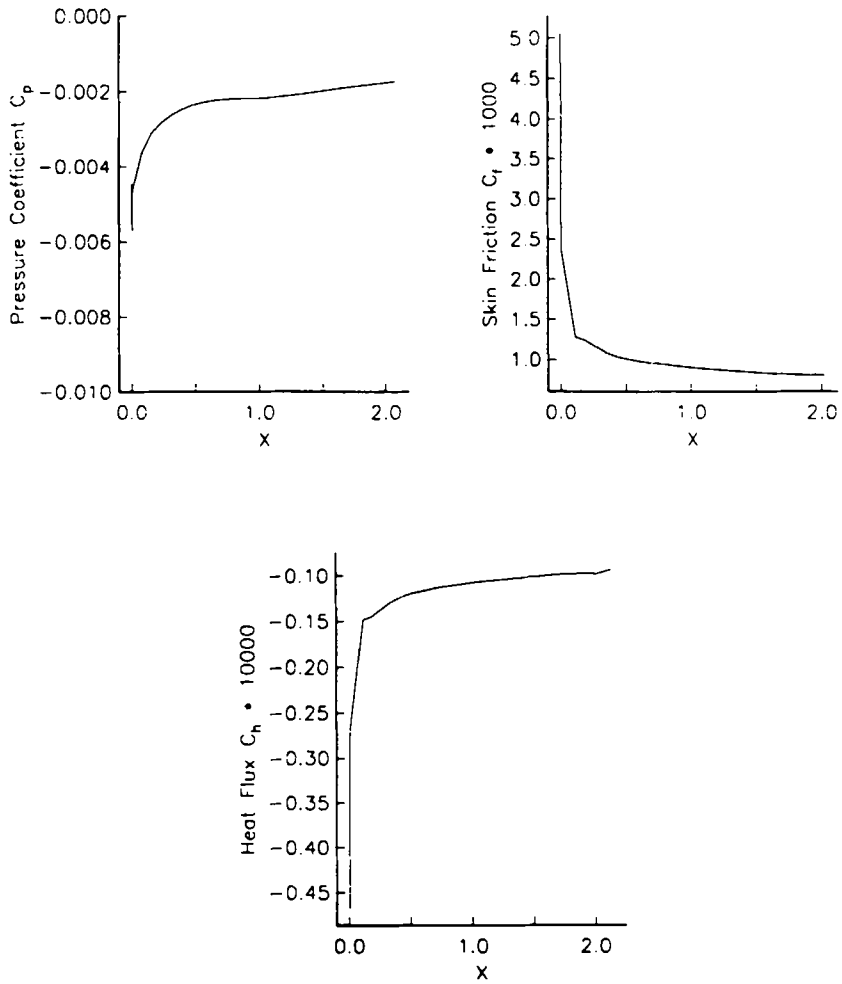

Figure 12

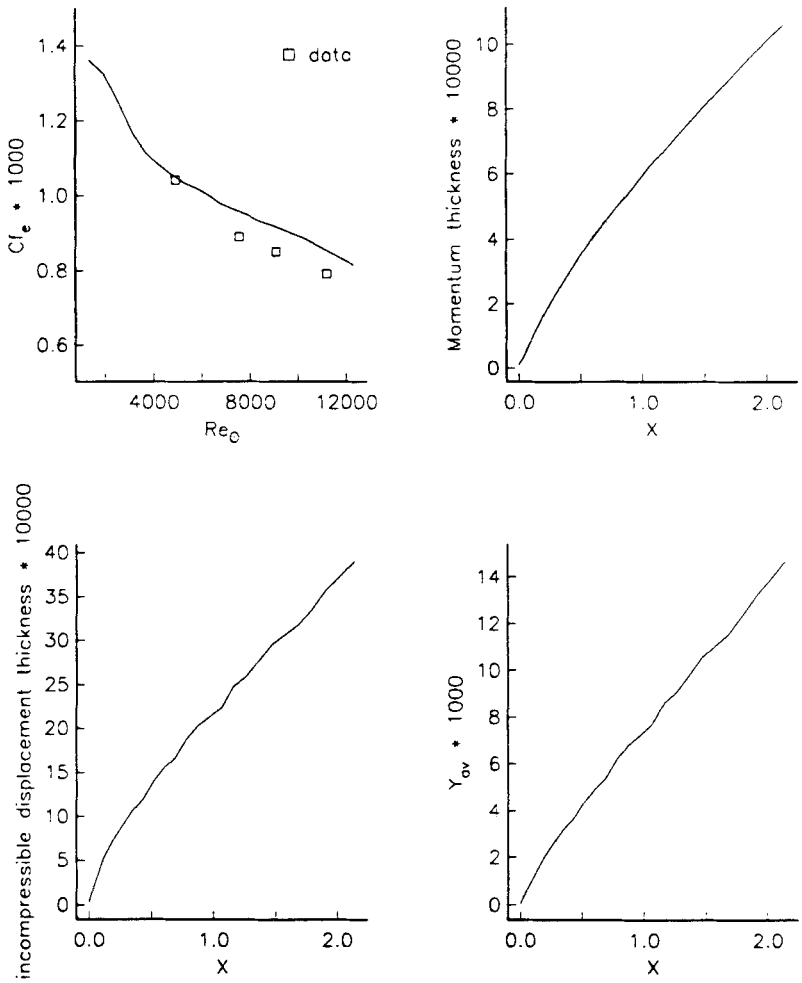

Figure 13

4. ALGEBRAIC MODELS FOR HIGH-SPEED SEPARATED FLOWS

It is well known that when the boundary layer becomes separated, both the Cebeci–Smith and the Baldwin–Lomax models give erroneous results because they rely on Prandtl's mixing-length theory, which is no longer relevant. This has been observed by many authors (see e.g. References 12 and 13) and is perhaps the major drawback of these models. Some improvement can be obtained by using the Cebeci–Smith model and by modifying the Van Driest damping factor,[12] but the results are still not very good in and downstream of the separated zone.

In 1986 Goldberg[14] proposed a new algebraic k–ε model to account for separated regions. His model is based on the following assumptions and observations on the separated region: the stress scale is given by the maximum shear stress in the separated layer, not by the wall stress; the shear layer has qualitatively the same turbulent structure when it is detached as when it is attached; and the length scale is the height of the separated region. Considering this and continuity arguments,

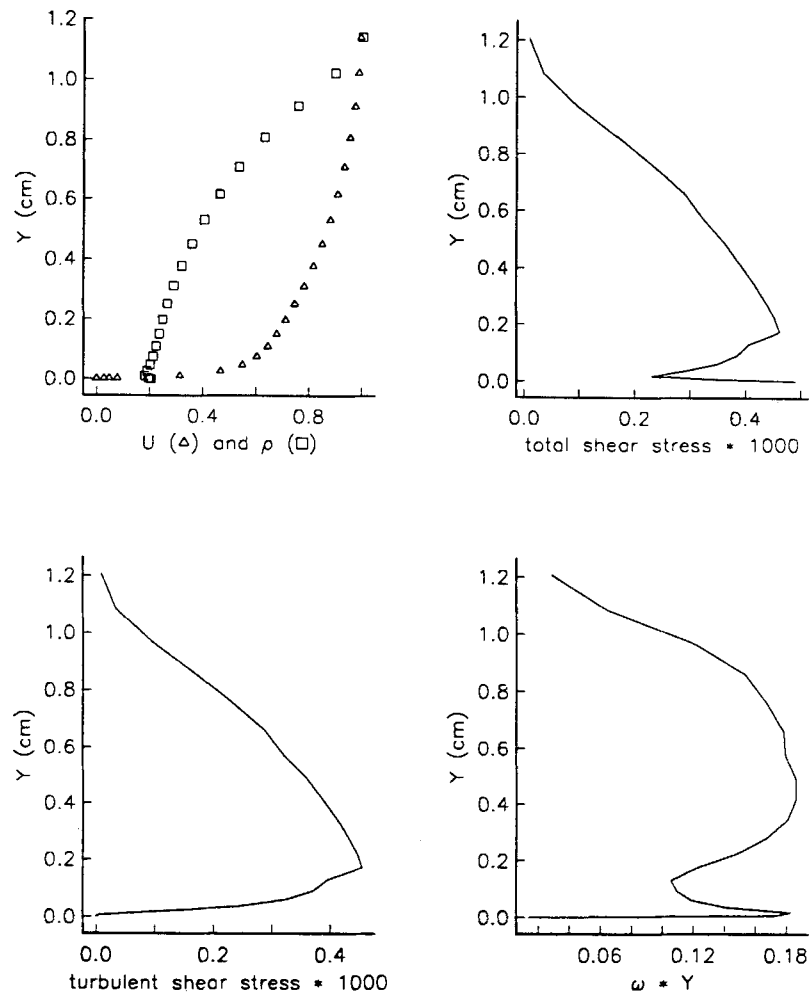

Figure 14

he proposed taking the kinetic energy of turbulence to be

$$k = k_b \frac{1-\exp[-\phi(y/y_b)^2]}{1-\exp(-\phi)}, \tag{27}$$

where the subscript 'b' refers to the backflow edge (defined by the point where the tangential speed is zero) and ϕ is a parameter, found empirically to be $\phi = 0{\cdot}5$.

The turbulence energy dissipation is taken to be

$$\varepsilon = k^{3/2}/y_b \tag{28}$$

because the length scale is y_b.

For high-Reynolds-number flows k_b can be taken to be (by analogy with the attached case)

$$k_b = u_s/\sqrt{C^*}, \tag{29}$$

where $C^* = 0{\cdot}09$ and

$$u_s = \sqrt{(-(u'v')_{\max})}.$$

Here $\overline{-(u'v')_{\max}}$ is the maximum turbulent shear stress, which occurs in the detached layer, and must be provided by the model used outside the separation bubble.

Altogether, the kinematic eddy viscosity is taken as

$$\nu_t = f(y)\left(\frac{k^2}{\varepsilon}\right)\sqrt{\left(\frac{\rho_w}{\rho}\right)} = C_1 u_s y_b \sqrt{\left(\frac{\rho_w}{\rho}\right)} f(y)\sqrt{(G(y))}, \tag{30}$$

where

$$f(y) = Ay/y_b + B. \tag{31}$$

The function f accounts for the laminar part in the vicinity of the wall. The constants A and B are found to be optimal at

$$A = -(C_\mu^*/2)^{9/5}, \qquad B = (C_\mu^*/2)^{3/5} - A, \qquad C_\mu^* = 0{\cdot}7.$$

The function G is the Gaussian

$$G(y) = \frac{1 - \exp[-\phi(y/y_b)^2]}{1 - \exp(-\phi)}. \tag{32}$$

Goldberg tested his model by computing a supersonic flow over a compression corner and obtained impressive results, including the correct prediction of separation and reattachment.[14]

To take separation into account, we will use the following blend of Cebeci's and Goldberg's models. In the attached regions we use the Cebeci model as described before, but replacing the wall shear stress in the Van Driest damping factor by the maximum shear stress in the profile to avoid an unphysical reduction of the eddy viscosity near separation and reattachment.

For separated profiles, consistently with Goldberg's hypothesis, we suppose that the shear layer is not qualitatively disturbed by the separation, so that we can take the eddy viscosity in it to be given by the Cebeci model, provided we use the distance to the backflow edge instead of the distance to the wall. In other words, μ_t is given by

$$\mu_t = \rho l^2 |\omega|, \qquad l = \kappa(y - y_b)\left[1 - \exp\left(-\frac{y - y_b}{A}\right)\right] \tag{33}$$

for $y_b \leqslant y \leqslant y_c$ and by

$$\mu_t = \alpha u_e \delta_i \left[1 + 5{\cdot}5\left(C_{KL}\frac{y - y_b}{y_{av}}\right)^6\right]^{-1} \tag{34}$$

for $y \geqslant y_c$, where

$$u_e\delta_i = \int_{y_b}^{y^*} y|\omega|\,dy, \tag{35}$$

$$y_{av} = \int_{y_b}^{y^*} y^2|\omega|\,dy \Big/ \int_{y_b}^{y^*} y|\omega|\,dy. \tag{36}$$

In the separation bubble, i.e. for $y \leqslant y_b$, we use Goldberg's model as described by (30).

The implementation of this model is no major problem in our framework, since we have well defined normals to the wall on which we can easily compute y_b, y^* and the integrals (35) and (36) giving $u_e\delta_i$ and y_{av}. The cost in terms of CPU time or storage is not significantly different for this

model as compared with the preceding one and remains very small (approximately 2% of the CPU time is used to compute the eddy viscosity).

Separation usually occurs at points where the solid wall is not convex; at these points the influences of the two convex components on one given fluid point are taken into account and averaged according to

$$\mu = \frac{d_2\mu_1 + d_1\mu_2}{d_1 + d_2}, \tag{37}$$

where the subscripts 1 and 2 refer to the two convex components of the wall and d is the normal distance to the wall.

The program automatically recognizes convexity defaults and performs the required averagings. The parts of the eddy viscosity depending on the different convex components are computed separately in order to allow vector processing; all this is completely geometry-independent assuming that the solid wall is locally convex.

As a preliminary test of this model, a high-speed moderate-Reynolds-number flow over a 15° compression corner was performed. The grid is shown in Figure 15; it has 2782 nodes and 5345 elements and was obtained by refining a Cartesian grid using an algorithm defined by Pouletty and Palmerio.[20,21] The shock is captured at the leading edge and the corner is at 1·39 m from the leading edge. The Reynolds number is $Re_\infty/m = 4{\cdot}95 \times 10^5$, the Mach number is $M_\infty = 5$, the free stream temperature is $T_\infty = 83{\cdot}6$ K and the temperature of the wall is $T_\infty = 288$ K. Figure 16 is a plot of the pressure. It can be seen that both the bow shock and the corner shock are captured neatly. In Figure 17 the pressure, skin friction and heat flux coefficients are plotted against the streamwise co-ordinate (the corner is at $x = 0$). The boundary layer experiences a small separation in the vicinity of the corner, after which the skin friction quickly recovers high values, as expected. Figure 18 is a plot of the ratio μ_t/μ of the eddy viscosity to the molecular viscosity. It varies between 0 and 15 between the leading edge and the corner; the flow in this region is first laminar

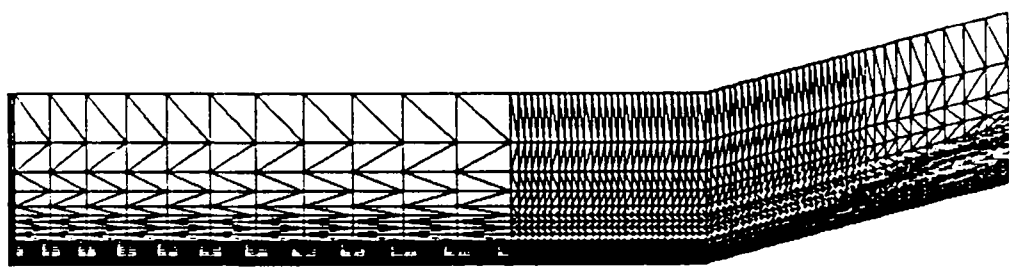

Figure 15

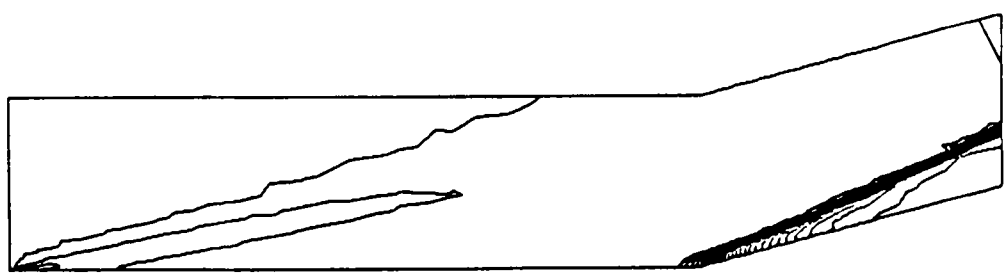

Figure 16

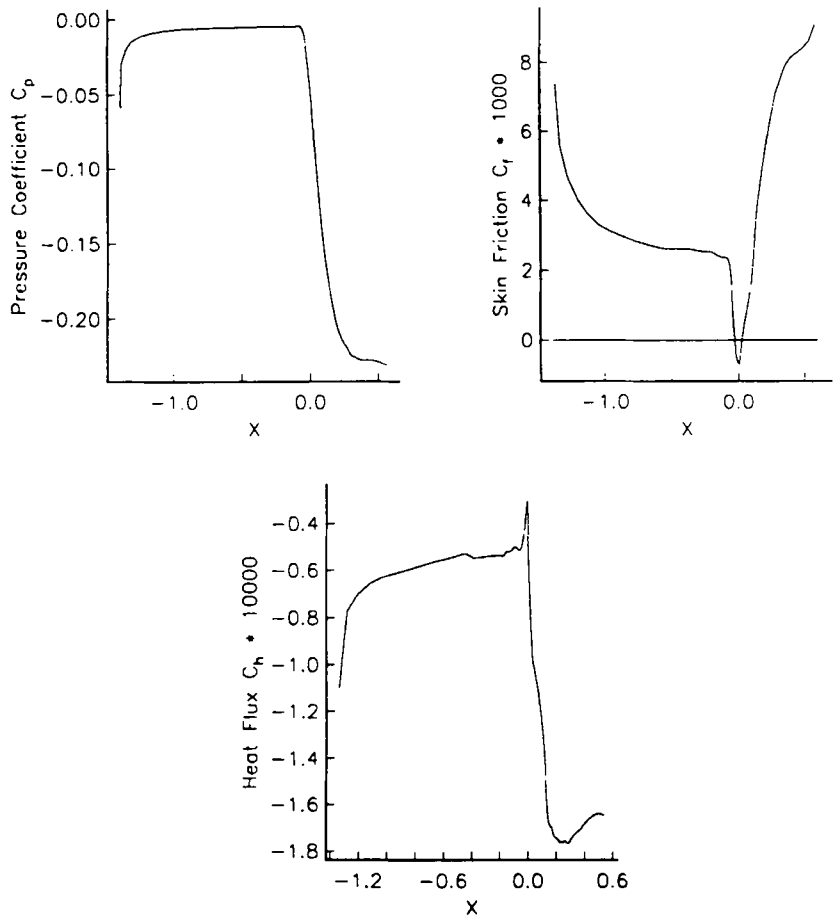

Figure 17

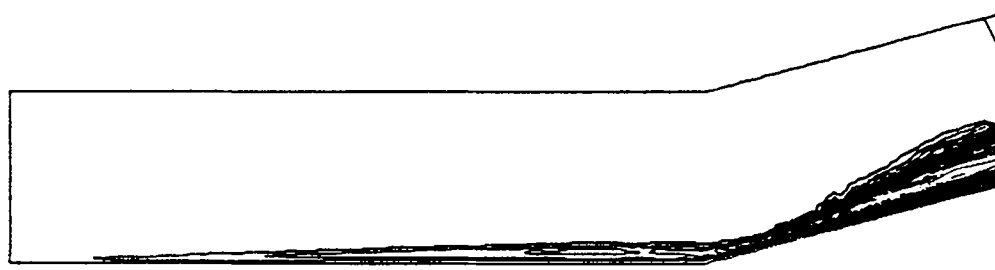

Figure 18

and then transitional. After the corner μ_t/μ increases quickly to values around 100, indicating a fully turbulent flow. Figures 19, 20 and 21 are plots of the velocity vectors at the corner, after separation and near the outflow respectively. Figure 22 shows profiles of speed, density and total and turbulent shear stress at the corner ($x = 0$). These profiles have the expected shape, although the discretization is maybe a bit coarse.

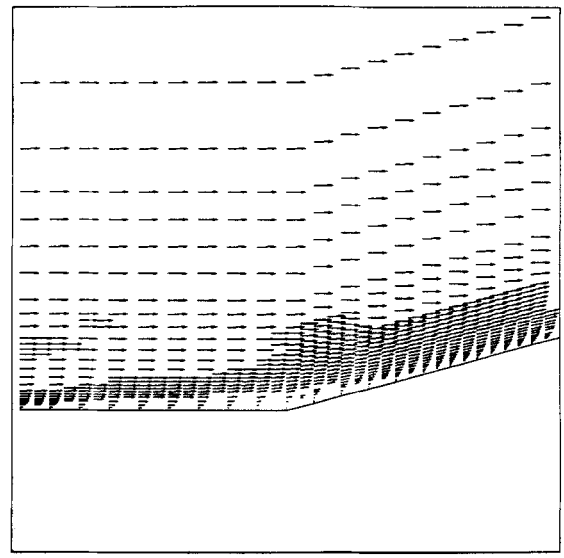

Figure 19

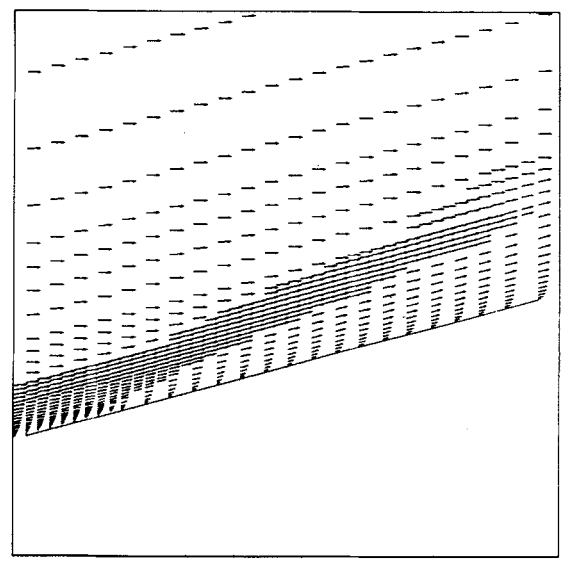

Figure 20

5. CONCLUSIONS

We have shown that algebraic turbulence models can be used in conjunction with unstructured grids at no major overcost in terms of either CPU time or storage. The program remains completely geometry-independent, which is consistent with the spirit of finite elements and unstructured grids.

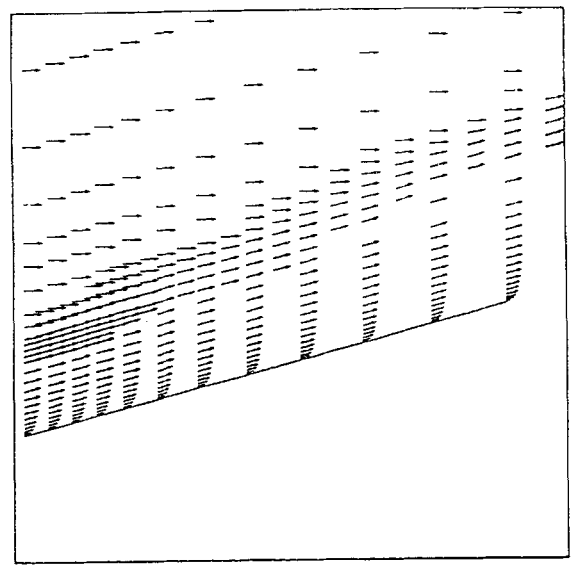

Figure 21

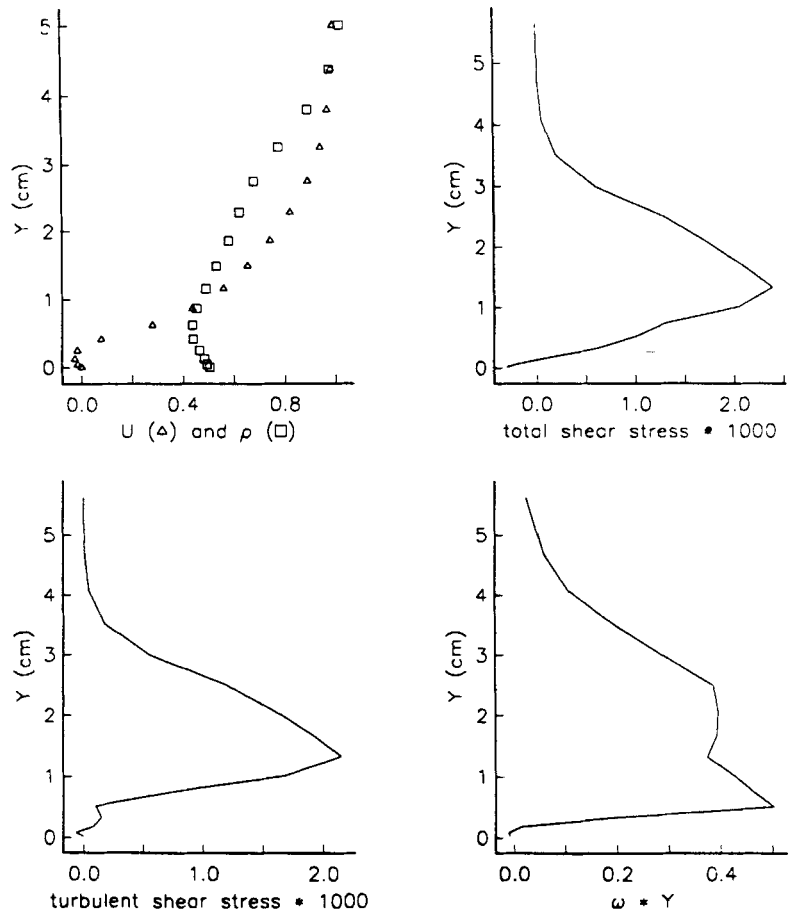

Figure 22

A practical way to use the Cebeci–Smith model has been proposed for both attached and separated flows; in the latter case Goldberg's modification has been used in the separated regions. The model has been shown to give accurate skin friction for high-speed zero-pressure-gradient boundary layers. A preliminary result for a separated flow is presented.

The major problem remaining to be solved before the model can be trusted to give even coarse results on real configurations is the transition region. Whether an *ad hoc* representation by switching the model off if the predicted value of the eddy viscosity is lower than a critical value, as suggested by Baldwin and Lomax,[11] would give a relevant result has not been investigated. More experimental data on transitional and/or separated high-speed flows are certainly necessary before answers can be given.

APPENDIX: NOMENCLATURE

C_f skin friction coefficient, $2\tau_w/\rho_\infty u_\infty^2$

C_h heat flux coefficient, $2q_w/\rho_\infty u_\infty^3$

C_p pressure coefficient, $2(p-p_\infty)/\rho_\infty u_\infty^2$

D deformation tensor, $D(\mathbf{u})=\nabla\mathbf{u}+\nabla\mathbf{u}^T-\frac{2}{3}\nabla\cdot\mathbf{u}I$

E total energy

I identity operator

k kinetic energy of turbulence

M Mach number

P Pressure

Pr Prandtl number, μ/λ

q heat flux

Re free stream Reynolds number, $\rho_\infty u_\infty/\mu_\infty$

Re_θ momentum thickness Reynolds number, $\rho_e u_e \theta/\mu_e$

T temperature

$\mathbf{u}$ velocity vector, $\mathbf{u}=(u, v)$

u component of the velocity tangent to the wall

u_s speed scale

$\mathbf{W}$ vector of conserved variables, $\begin{pmatrix}\rho\\ \rho u\\ \rho v\\ E\end{pmatrix}$

x co-ordinate tangent to the wall

y co-ordinate normal to the wall

α Clauser's constant, $\alpha=0{\cdot}0168$

δ boundary layer thickness defined by $u/u_e=0{\cdot}99$

δ^* displacement thickness, $\int_0^\delta (1-\rho u/\rho_e u_e)\,dy$

δ_i incompressible displacement thickness $\int_0^\delta (1-u/u_e)\,dy$

ε isotropic part of turbulence energy dissipation

λ heat conductivity

μ molecular viscosity

κ Von Karman's constant, $\kappa=0{\cdot}4$

ν	kinematic viscosity, μ/ρ
ω	vorticity
∇	gradient operator
$\nabla\cdot$	divergence operator

Subscripts

b	at backflow edge
e	at boundary layer edge
i	at streamwise position $i\Delta x$
j	at crossflow position $j\Delta y$
t	turbulent
w	at wall
∞	free stream conditions

Superscripts

′	fluctuating quantities
$\bar{}$	averaged
T	transpose

ACKNOWLEDGEMENTS

This research was supported by the National Aeronautics and Space Administration under NASA Contract No. NAS1-18107 while the author was in residence at the Institute for Computer Applications in Science and Engineering (ICASE), NASA Langley Research Center, Hampton, VA 23665, U.S.A. Additional support was also provided under DRET Contract No. 03407901.

REFERENCES

1. G. V. Candler and R. W. MacCormack, 'Hypersonic flow past 3D configurations', *AIAA 87-0480*, Reno, 12–16 January 1987.
2. S. Chakravarthy, 'High resolution upwind formulations for the Navier–Stokes equations', *Von Karman Institute Lecture Series, 1988-05*, 7–11 March 1988.
3. A. Jameson and H. Rieger, 'Solution of steady three dimensional compressible Euler and Navier–Stokes equations by an implicit LU scheme', *AIAA 88-0619*, Reno, 1988.
4. B. Stoufflet and L. Fezoui, 'A class of implicit upwind schemes for Euler simulations with unstructured meshes', *Journal of Computational Physics*, to appear.
5. B. Stoufflet, J. Periaux, L. Fezoui and A. Dervieux, 'Numerical simulations of 3D hypersonic Euler flows around space vehicles using adapted finite elements', *AIAA 87-0560*, Reno, January 1987.
6. S. Osher and F. Solomon, 'Upwind difference schemes for the hyperbolic systems of conservation laws', *Math. Comput.* **38,** 339–374 (1982).
7. P. Rostand and B. Stoufflet, 'TVD schemes to compute compressible viscous flows on unstructured meshes', *Proc. 2nd Int. Conf. on Hyperbolic Problems*, Aachen, Vieweg, 1988.
8. C. G. Speziale, 'On nonlinear K–l and K–ε models of turbulence', *J. Fluid Mech.*, **178,** 459–475 (1987).
9. J. Shang and W. L. Hankey, 'Numerical solution of supersonic turbulent flow over a compression ramp', *AIAA J.*, **13,** 1368–1374 (1975).
10. T. Cebeci and A. Smith, *Analysis of Turbulent Boundary Layers*, Academic Press, New York, 1974.
11. B. S. Baldwin and H. Lomax, 'Thin layer approximation and algebraic model for separated turbulent flows', *AIAA 78-257*, Huntsville, 16–18 January 1978.
12. M. Visbal and D. Knight, 'The Baldwin–Lomax turbulence model for two-dimensional shock-wave/boundary layer interactions', *AIAA J.*, **22,** 921–928 (1984).
13. B. York and D. Knight, 'Calculation of a class of two dimensional turbulent boundary layer flows using the Baldwin–Lomax model', *AIAA 85-0126*, Reno, January 1985.
14. U. C. Goldberg, 'Separated flow treatment with a new turbulence model', *AIAA J.*, **24,** 1711–1713 (1986).

15. E. J. Hopkins, E. R. Keener, T. E. Poleh and H. A. Dwyer, 'Hypersonic turbulent skin-friction and boundary layer profiles on nonadiabatic flat plates', *AIAA J.*, **10**, 40–48 (1972).
16. M. Mallet, J. Periaux, P. Perrier and B. Stoufflet, 'Flow modelization and computational methodologies for the aerothermal design of hypersonic vehicles: application to the European Hermes', *AIAA 88-2628*, San Antonio, June 1988.
17. F. el Dabaghi, *Thesis*, Universite Paris XIII, 1984.
18. P. S. Klebanoff, 'Characteristics of turbulence in a boundary layer with zero pressure gradient', *NACA TN 3178*, 1954.
19. C. C. Sun and M. E. Childs, 'A modified wall wake velocity profile for turbulent compressible boundary layers', *J. Aircraft*, **10**, 381–383 (1973).
20. C. Pouletty, 'Generation et optimisation de Maillages en elements finis, application à la résolution des équations de la mécanique des fluides', *Thèse de Docteur Ingenieur*, Ecole Centrale, December 1985.
21. B. Palmerio, 'Self adaptive FEM algorithms for the Euler equations', *INRIA Report 338*, 1985.